Skeletal Radiology (2022) 51:1853–1863
https://doi.org/10.1007/s00256-022-04040-6

SCIENTIFIC ARTICLE

Reliability and benefits of single-energy projection-based metallic artifact reduction (SEMAR) in the different orthopedic hardware for the hip

Yu-Hua Chen[1] · Chia-Hsin Lu[1,2,3] · Yu-Jen Chen[2,3] · Han-Sheng Chen[2,3] · Tsyh-Jyi Hsieh[3,4]

Received: 6 December 2021 / Revised: 20 March 2022 / Accepted: 21 March 2022 / Published online: 26 March 2022

Abstract

Objective To evaluate the performance and reliability of the single-energy metal artifact reduction (SEMAR) algorithm in patients with different orthopedic hardware at the hips.

Materials and methods A total of 153 patients with hip instrumentation who had undergone CT with adaptive iterative dose reduction (AIDR) 3D and SEMAR algorithms between February 2015 and October 2019 were included retrospectively. Patients were divided into 5 groups by the hardware type. Two readers with 21 and 13 years of experience blindly reviewed all image sets and graded the extent of artifacts and imaging quality using 5-point scales. To evaluate reliability, the mean densities and image noises were measured at the urinary bladder, veins, and fat in images with artifacts and the reference images.

Results No significant differences were found in the mean densities of the urinary bladder, veins, and fat between the SEMAR images with artifacts (7.57 ± 9.49, 40.29 ± 23.07, 86.78 ± 38.34) and the reference images (7.77 ± 6.2, 40.27 ± 8.66, 89.10 ± 20.70) ($P = .860$, $.994$, $.392$). Image noises of the urinary bladder in the SEMAR images with artifacts (14.25 ± 4.50) and the SEMAR reference images (9.69 ± 1.29) were significantly higher than those in the AIDR 3D reference images (9.11 ± 1.12) ($P < .001$; $P < .001$). All AIDR 3D images were non-diagnostic (overall quality ≤ 3) and less than a quarter of the SEMAR images were non-diagnostic (16.7–23.7%), mainly in patients with prostheses [reader 1: 91.7% (22/24); reader 2: 92.6% (25/27)].

Conclusion The SEMAR algorithm significantly reduces metal artifacts in CT images, more in patients with internal fixations than in patients with prostheses, and provides reliable attenuation of soft tissues.

Keywords Computed tomography (CT) · Metal artifact · Metal artifact reduction · Orthopedic hardware · Hip

Introduction

Hip fracture is an important and common public health issue that increases morbidity and mortality in older adults [1]. Surgery using orthopedic hardware such as arthroplasty and internal fixation is recommended to improve outcomes in patients with hip fractures [2]. Although radiographs are the first-line modality for evaluation of the orthopedic hardware at the hips, computed tomography (CT) provides excellent evaluation of both bone and soft tissue pathology [3]. However, the metal orthopedic hardware is problematic in the follow-up CT scans because it causes beam hardening that decreases the imaging quality and loss of information about underlying structures [4, 5]. To improve diagnostic accuracy, the reduction of metal artifacts has become an important issue in modern CT systems [5, 6].

✉ Tsyh-Jyi Hsieh
tsyhjyi.hsieh@gmail.com

1 Department of Medical Imaging, Kaohsiung Municipal Ta-Tung Hospital, Kaohsiung Medical University Hospital, Kaohsiung Medical University, Kaohsiung, Taiwan

2 Department of Medical Imaging, Kaohsiung Medical University Hospital, Kaohsiung Medical University, Kaohsiung, Taiwan

3 Department of Radiology, Faculty of Medicine, College of Medicine, Kaohsiung Medical University, Kaohsiung, Taiwan

4 Department of Medical Imaging, Chi Mei Medical Center, No.901, Zhonghua Rd, Yongkang Dist, Tainan City 710, Taiwan

Traditionally, adjusting acquisition parameters such as increased tube current and voltage are used but the effect of reducing metal artifacts is limited [4, 6]. After the invention of dual-energy CT techniques, virtual monochromatic images, especially at high energy levels, can provide better imaging quality with less beam hardening [5, 7, 8]. However, dual-energy CT is expensive and there is less tissue contrast in the virtual monochromatic images at high energy levels [9, 10]. Recently, because of the advancement of computers in complex calculations, several projection-based metal artifact reduction algorithms that can be applied on the single-energy CT are introduced by CT vendors are able to provide better imaging quality than the traditional methods [5, 6, 11]. The single-energy metal artifact reduction (SEMAR) algorithm is one such algorithm and is reported to dramatically reduce metal artifacts and improve imaging quality have been reported [12–15]. Nevertheless, the reliability of the measurement of CT densities at the underlying structures, which is important in the evaluation of soft tissue pathology, has not been well defined. Furthermore, previous studies have focused on the reduction effect for hip arthroplasty with large metal compartments, which caused unresolvable artifacts using the traditional methods [13–15]. Thorough investigation of the effects of the SEMAR algorithm in the reduction of metal artifacts from different metal hardware is lacking.

In this study, we compared the image quality of CT with iterative reconstruction (IR) alone and in association with a SEMAR algorithm in postoperative patients with different orthopedic hardware at the hips. The study purpose was to evaluate the performance of the SEMAR algorithm in patients with different orthopedic hardware at the hips and the reliability of measured densities at specific periarticular soft tissue structures.

Materials and methods

Patient population

Patients with hip instrumentation who had undergone a routine CT, including the pelvic region, at a single institution between February 2015 and October 2019 ($n = 153$) were enrolled in this retrospective study. The inclusion criteria were adults with complete routine CT using helical scans with the adaptive iterative dose reduction (AIDR) 3D algorithm for the entire study region and volume scans with the SEMAR algorithm for the hip instrumentation region. The exclusion criteria were significant motion artifacts in any one of the scans. Based on the different types of orthopedic hardware, patients were then divided into 5 groups: bilateral prostheses, unilateral prosthesis, bilateral internal osteosynthesis fixation (IF), unilateral IF, and prosthesis + IF (prosthesis at one hip and IF at another hip).

Ethical considerations

This retrospective study was approved by the local institutional review board of our hospital. Because the images were deidentified and patients remained anonymous, the requirement to obtain informed consent was waived.

CT image acquisition

All included patients were scanned using a 640-MDCT scanner (Aquilion One, Version V6.0, Canon Medical Systems, Otawara, Tochigi, Japan). The scan parameters of the helical scan with the AIDR 3D algorithm (Canon Medical Systems, Otawara, Tochigi, Japan) were helical acquisition; detector collimation, 80 rows × 0.5 mm; tube

Table 1 Patient and implant characteristics

	N (%)	Age (years)	Female	$CTDI_{vol}$ (mGy)		*P**
				AIDR 3D	SEMAR	
Total	153	75.52 ± 13.70	93	11.32 ± 4.32	10.98 ± 4.11	.013[†]
IF bilateral	8 (5.2)	83.25 ± 8.19	8	10.35 ± 4.69	9.18 ± 4.50	.120
IF unilateral	42 (27.5)	74.64 ± 13.00	24	12.30 ± 4.24	11.45 ± 3.91	.002[#]
Prosthesis bilateral	25 (16.3)	74.24 ± 18.01	15	11.65 ± 4.7	12.00 ± 4.39	.292
Prosthesis unilateral	67 (43.8)	75.57 ± 13.17	42	10.83 ± 4.31	10.56 ± 4.12	.188
Prosthesis + IF	11 (7.2)	75.91 ± 11.64	4	10.53 ± 3.35	10.74 ± 3.73	.542

*The *P* value for the comparison of mean $CTDI_{vol}$ between AIDR 3D and SEMAR

[†]Statistically significant ($P < .05$)

[#]Statistically significant ($P < .01$)

AIDR 3D, adaptive iterative dose reconstruction algorithm; *SEMAR*, single-energy metal artifact reduction algorithm; *IF*, internal fixation; *$CTDI_{vol}$*, volume computed tomography dose index

Table 2 Mean attenuation and noise of the images with artifacts and the reference images of AIDR 3D and SEMAR reconstruction

	AIDR 3D with artifacts	AIDR 3D reference	SEMAR with artifacts	SEMAR reference	P^a	P^b	P^c	P^d	P^e	P^f
Attenuation (HU)										
Urinary bladder ($n=39$)	−4.09 ± 30.22	8.87 ± 7.12	7.57 ± 9.49	7.77 ± 6.2	.008*	.006*	.007*	.323	.147	.860
Vein ($n=153$)	106.65 ± 82.20	40.33 ± 6.92	40.29 ± 23.07	40.27 ± 8.66	< .001*	< .001*	< .001*	.982	.935	.994
Fat ($n=153$)	− 170.14 ± 84.53	−91.55 ± 31.76	− 86.78 ± 38.34	−89.10 ± 20.70	< .001*	< .001*	< .001*	.155	.223	.392
Noise (HU)										
Urinary bladder ($n=39$)	39.61 ± 45.30	9.11 ± 1.12	14.25 ± 4.50	9.69 ± 1.29	< .001*	0.001*	< .001*	< .001*	< .001*	< .001*
Vein ($n=153$)	19.75 ± 13.55	9.30 ± 2.74	13.43 ± 9.32	10.69 ± 2.71	< .001*	< .001*	< .001*	< .001*	< .001*	< .001*
Fat ($n=153$)	34.55 ± 19.22	18.65 ± 2.77	21.31 ± 5.85	20.03 ± 3.09	< .001*	< .001*	< .001*	< .001*	< .001*	.011*

[a] *P* value for AIDR 3D images with artifacts versus AIDR 3D reference images

[b] *P* value for AIDR 3D images with artifacts versus SEMAR images with artifacts

[c] *P* value for AIDR 3D images with artifacts versus SEMAR reference images

[d] *P* value for AIDR 3D reference images versus SEMAR images with artifacts

[e] *P* value for AIDR 3D reference images versus SEMAR reference images

[f] *P* value for SEMAR images with artifacts versus SEMAR reference images

* Statistically significant ($P < .0125$)

AIDR 3D, adaptive iterative dose reconstruction algorithm; *SEMAR*, single-energy metal artifact reduction algorithm

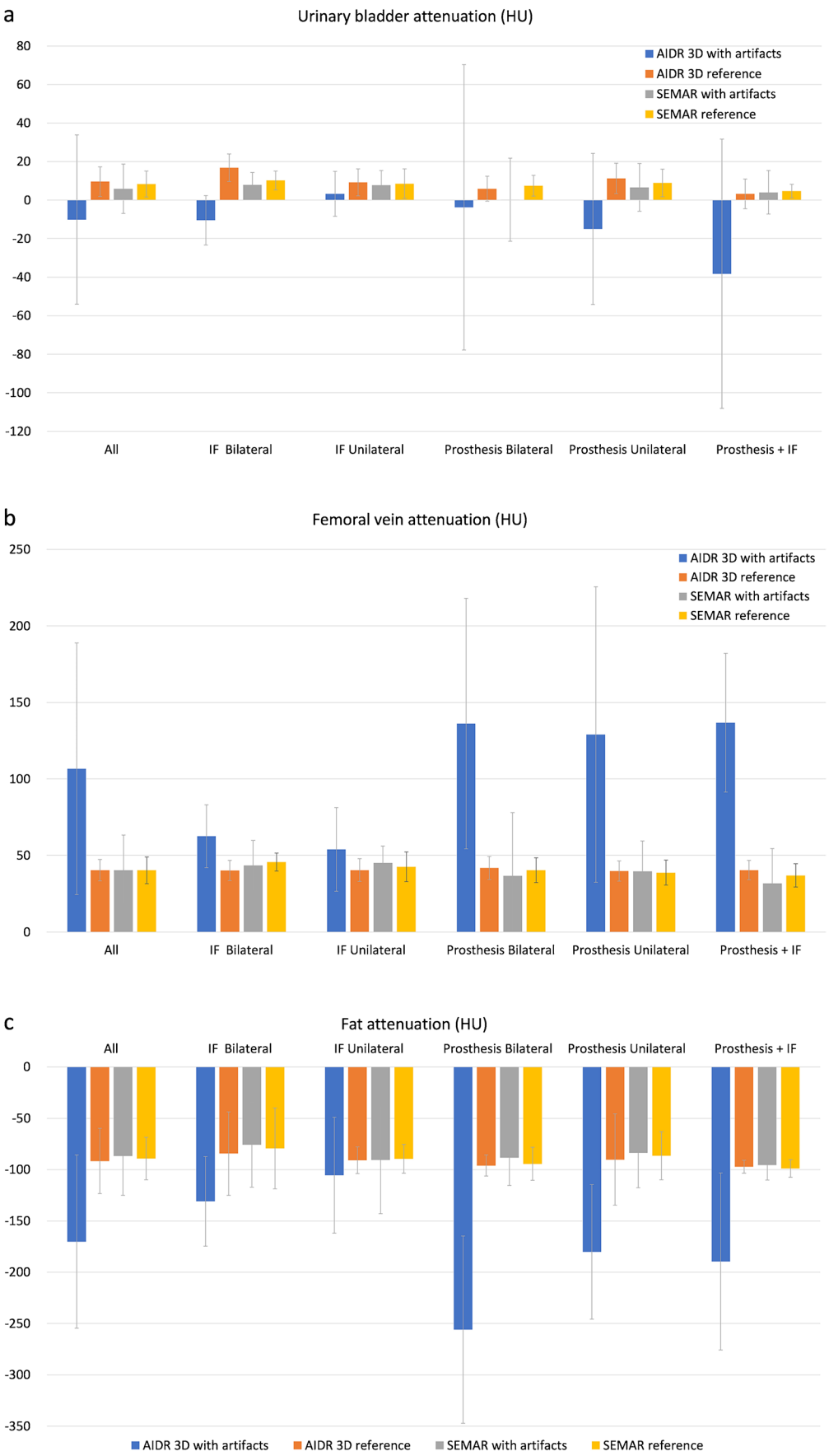
a
Urinary bladder attenuation (HU)
80
60
40
20
0
-20
-40
-60
-80
-100
-120
AIDR 3D with artifacts
AIDR 3D reference
SEMAR with artifacts
SEMAR reference
All
IF Bilateral
IF Unilateral
Prosthesis Bilateral
Prosthesis Unilateral
Prosthesis + IF
b
Femoral vein attenuation (HU)
250
200
150
100
50
0
AIDR 3D with artifacts
AIDR 3D reference
SEMAR with artifacts
SEMAR reference
All
IF Bilateral
IF Unilateral
Prosthesis Bilateral
Prosthesis Unilateral
Prosthesis + IF
c
Fat attenuation (HU)
All
IF Bilateral
IF Unilateral
Prosthesis Bilateral
Prosthesis Unilateral
Prosthesis + IF
0
-50
-100
-150
-200
-250
-300
-350
AIDR 3D with artifacts
AIDR 3D reference
SEMAR with artifacts
SEMAR reference

◂**Fig. 1** Mean and standard deviation of attenuations at **a** the urinary bladder, **b** common femoral vein, and **c** subcutaneous fat were recorded by different types of hardware

rotation time, 0.5 s; tube voltage, 120 kV; tube current, 300–550 mA (automatic exposure control); and helical pitch factor, 0.813. The scan parameters of the volume scan with the SEMAR algorithm (Canon Medical Systems, Otawara, Tochigi, Japan) were sequential acquisition; detector collimation, 280–320 rows × 0.5 mm; tube rotation time, 0.5 s; tube voltage, 120 kV; and tube current, 300–550 mA (automatic exposure control). The volume CT dose index ($CTDI_{vol}$) of each scan was recorded.

Image reconstruction

The CT images were reconstructed as 5.0 mm sections at 0.0 mm intervals for the helical and volume scans. The helical scans were reconstructed by using an AIDR 3D algorithm and the volume scans by using an AIDR 3D with the SEMAR algorithm. A standard soft tissue kernel (FC08) was used for all reconstructions.

Preparation for image evaluation

Before being reviewed, all images were randomly assigned a new identification number, and the original identification numbers, patients' names, and study descriptions were erased by a radiographer with 10 years of experience. To evaluate the influence of the metallic devices, axial images with the most obvious metallic artifacts (images with artifacts) were selected for qualitative and quantitative evaluations by one radiographer with 12 years of experience. Axial images 1 cm above the top of orthopedic hardware were selected as reference images by the same radiologist.

Quantitative image analysis

The following regions of interest (ROIs) were drawn 3 times in AIDR 3D and SEMAR images on the images with artifacts and the reference images, including the common femoral vein and subcutaneous fat at the lateral aspect of the hip ipsilateral to the hardware and the urinary bladder. In patients with hardware at the bilateral hip, the ROIs were drawn at the side with more artifacts or at the right hip region if the artifacts were about the same. The average mean attenuations (HU) in the ROI were analyzed to evaluate reliability. The average standard deviation (SD) of the attenuation in the ROI was set as the image noise.

Qualitative image analysis

The images with artifacts were evaluated independently by two radiologists with 21 and 13 years of experience, respectively, who were blinded to the reconstruction methods. To prevent recall bias, the radiologists reviewed axial images of the different sequences at separate times at least 1 month apart. The images were reviewed using the standard picture archiving and communication system (EBM-viewer, EBM, Taiwan) on the standard viewer stations (dual 5 million-pixel monitors) in the study hospital. The windows width and level were fixed at 350 and 50 Hounsfield units (HU), respectively.

To evaluate overall quality, a 5-point scale was used to grade images by the severity of metal artifacts, as follows: 1, severe artifacts causing poor recognition of pelvic organs and muscles; 2, moderate artifacts causing partially obscured pelvic organ (urinary bladder or prostate) (< 50%) and muscles (< 50%); 3, some artifacts causing faint recognition of pelvic organ and poor recognition of periarticular soft tissue; 4, mild artifacts with good recognition of pelvic organs and periarticular soft tissue; and 5, minimal to no artifacts. To evaluate visibility of the pelvic organs, muscles, and common femoral vessels, a 5-point scale was used to grade images, as follows: 1, severely obscured (> 50%); 2, partially obscured (20–50%); 3, slightly obscured pelvic organs (< 20%); 4, visible with some heterogeneous densities; and 5, nearly normal imaging. Under consideration of good recognition of both pelvic organs and periarticular soft tissue, scales 4 and 5 were considered as diagnostic images.

To evaluate the image quality of SEMAR in the reference images, the readers compared the AIDR 3D images and SEMAR images side by side and graded them using a 5-point scale, as follows: − 2, significantly better quality on AIDR 3D images than SEMAR images; − 1, mildly better quality on AIDR 3D images; 0, similar quality between AIRDR 3D and SEMAR images; 1, mildly poorer quality on AIDR 3D images; and 2, significantly poorer quality on AIDR 3D images.

Statistical analysis

Statistical analysis was performed by using the Statistical Package for Social Science (SPSS) version 20 (IBM SPSS Statistics, Chicago, IL, USA). Distributions of qualitative and quantitative evaluation for image quality of the different hardware types were analyzed. Differences between the images with artifacts and the reference images of the AIDR 3D and SEMAR algorithm were evaluated using the paired *t*-test and $P < 0.0125$ (0.05/4) was considered statistically significant. Side-by-side comparisons between AIDR 3D images and SEMAR images were evaluated using a one-sample *t*-test. $P < 0.05$ was considered statistically

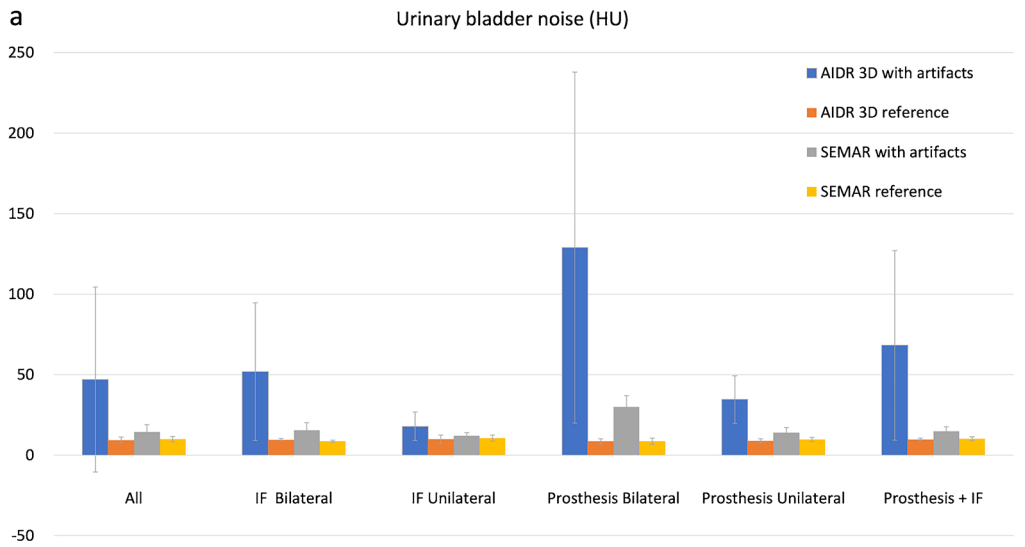
a
Urinary bladder noise (HU)
250
200
150
100
50
0
-50
AIDR 3D with artifacts
AIDR 3D reference
SEMAR with artifacts
SEMAR reference
All
IF Bilateral
IF Unilateral
Prosthesis Bilateral
Prosthesis Unilateral
Prosthesis + IF

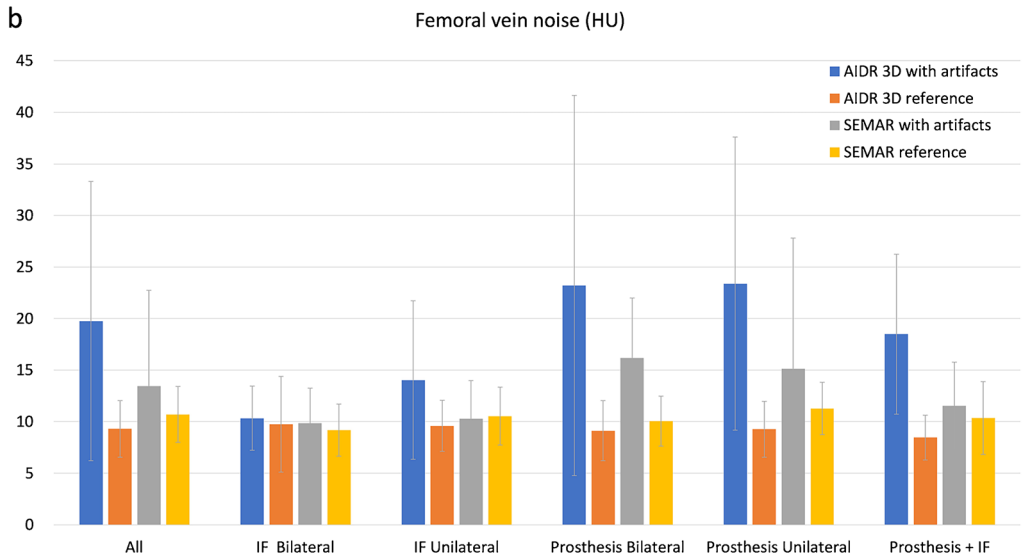
b
Femoral vein noise (HU)
45
40
35
30
25
20
15
10
5
0
AIDR 3D with artifacts
AIDR 3D reference
SEMAR with artifacts
SEMAR reference
All
IF Bilateral
IF Unilateral
Prosthesis Bilateral
Prosthesis Unilateral
Prosthesis + IF

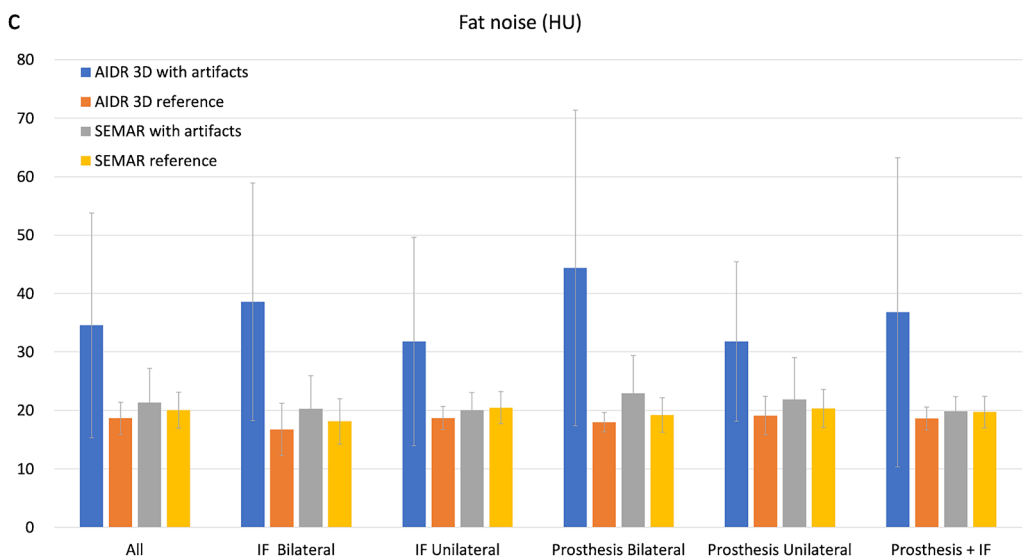
c
Fat noise (HU)
80
70
60
50
40
30
20
10
0
AIDR 3D with artifacts
AIDR 3D reference
SEMAR with artifacts
SEMAR reference
All
IF Bilateral
IF Unilateral
Prosthesis Bilateral
Prosthesis Unilateral
Prosthesis + IF

◂**Fig. 2** Mean and standard deviation of noises at **a** the urinary bladder, **b** common femoral vein, and **c** subcutaneous fat were recorded by different types of hardware

significant in the analysis of all images. Differences in the qualitative evaluation between the different hardware types were evaluated using one-way ANOVA with Tukey's post-tests and $P < 0.01$ (0.05/5) was considered statistically significant. The inter-rater correlation coefficients were examined using the kappa statistic. $P < 0.05$ was considered statistically significant. Poor, fair, moderate, good, and excellent agreement corresponded to the following ranges of kappa values: 0.00–0.20, 0.21–0.40, 0.41–0.60, 0.61–0.80, and 0.81–1.00, respectively.

Results

A total of 153 patients (93 females; mean age 75.5, range 32–97 years) with hardware at the hip joints were enrolled in this study. Table 1 shows patients' demographic data and distribution of the different types of hardware. Mean $CTDI_{vol}$ value of the SEMAR images was significantly lower than that of the AIDR 3D images in all patients ($P = 0.013$) and in the unilateral IF group ($P = 0.002$).

Quantitative image analysis

In the images with artifacts, the urinary bladder was measured in 113 patients. The mean attenuation achieved with AIDR 3D images (-10.12 ± 43.93 HU) was significantly lower than that achieved with SEMAR images (5.92 ± 12.86 HU) ($P < 0.001$). Data of the veins and fat were measured in images with artifacts and reference images in all patients and only 39 patients had measurable data at the urinary bladder in both artifacts and reference images. The mean attenuations of the urinary bladder, veins, and fat in the AIDR 3D images with artifacts were significantly lower than those in the AIDR 3D reference images ($P = 0.008$, $P < 0.001$, $P < 0.001$), in SEMAR images with artifacts ($P = 0.006$, $P < 0.001$, $P < 0.001$), and in SEMAR reference images ($P = 0.007$, $P < 0.001$, $P < 0.001$) (Table 2). No significant differences were seen in the mean attenuations of the urinary bladder, veins, and fat between the SEMAR images with artifacts and the SEMAR reference images (all $P > 0.05$). Figure 1 shows the distribution of the attenuations of the urinary bladder, veins, and fat in patients with different types of hardware.

In images with artifacts, the mean noise of the urinary bladder in the AIDR 3D images (-46.93 ± 57.41 HU) was significantly lower than that in the SEMAR images (14.41 ± 4.45 HU) ($P < 0.001$). Comparison of images with artifacts and reference images revealed that the mean noise of the urinary bladder in AIDR 3D images with artifacts was significantly higher than those in AIDR 3D reference images ($P < 0.001$), in SEMAR images with artifacts ($P < 0.001$), and in SEMAR reference images ($P < 0.001$) (Table 2). The mean noises of the urinary bladder in SEMAR images with artifacts and SEMAR reference images were significantly higher than that in AIDR 3D reference images ($P < 0.001$; $P < 0.001$). Figure 2 shows the distribution of the noises of the urinary bladder, veins, and fat in the patients with different types of hardware.

Qualitative image analysis

The detailed results of qualitative image analyses in the images with artifacts are shown in Table 3. All AIDR 3D images were non-diagnostic (overall quality ≤ 3) and about one-sixth of the SEMAR images were non-diagnostic (15.7–17.6%), mainly in patients with prostheses, including bilateral prostheses, unilateral prostheses, and IF + prostheses [reader 1: 91.7% (22/24); reader 2: 92.6% (25/27)] (Fig. 3). Scores of the overall quality and the visibilities of pelvic organ muscles and vessels in the SEMAR images were significantly higher than those in the AIDR 3D images in all patients and subgroups with different types of hardware (all $P < 0.001$) (Fig. 4). Non-diagnostic images (overall quality ≤ 3) in SEMAR images were noted in the subgroups of unilateral IF [reader 1: 4.8% (2/42); reader 2: 4.8% (2/42)], bilateral prostheses [reader 1: 44.0% (11/25); reader 2: 48.0% (12/25)], unilateral prostheses [reader 1: 13.4% (9/67); reader 2: 16.4% (11/67)], and prosthesis + IF [reader 1: 18.2% (2/11); reader 2: 18.2% (2/11)] (Fig. 5). In analyzing differences between different types of hardware (Fig. 6), scores of the overall quality, visibility of pelvic organs, and visibility of vessels were significantly higher in the unilateral IF group than in those of the bilateral prostheses, unilateral prosthesis, and prosthesis + IF groups (all $P < 0.01$ for two readers). The mean score of the visibility of muscles of the unilateral IF group was also significantly higher than those of the bilateral prostheses and unilateral prosthesis groups (all $P < 0.01$ for two readers). However, no significant differences were found in scores between the other different types of hardware.

The inter-rater correlation coefficients, indicators of inter-rater reliability, were 0.86 (95% CI: 0.79 to 0.93, $P < 0.001$) and 0.86 (95% CI: 0.79 to 0.93, $P < 0.001$) for the overall quality scores of the AIDR 3D images and SEMAR images, respectively; 0.80 (95% CI: 0.72 to 0.87, $P < 0.001$) and 0.92 (95% CI: 0.86 to 0.98, $P < 0.001$) for the visibility of pelvic organs in the AIDR 3D images and SEMAR images, respectively; 0.83 (95% CI: 0.75 to 0.91, $P < 0.001$) and 0.81 (95% CI: 0.73 to 0.89, $P < 0.001$) for the visibility of muscles in the AIDR 3D images and SEMAR images, respectively; and

Table 3 Subjective analysis of image quality of the AIDR 3D and SEMAR reconstructions

Number (1/2/3/4/5)	Total	IF bilateral	IF unilateral	Prosthesis bilateral	Prosthesis unilateral	Prosthesis + IF
Overall quality						
Reader 1						
AIRD 3D	49/66/38/0/0	2/5/1/0/0	0/10/32/0/0	25/0/0/0/0	14/48/5/0/0	8/3/0/0/0
SEMAR	0/4/20/84/45	0/0/0/5/3	0/1/1/11/29	0/0/11/14/0	0/3/6/46/12	0/0/2/8/1
Reader 2						
AIRD 3D	43/70/40/0/0	2/5/1/0/0	0/6/36/0/0	23/2/0/0/0	10/54/3/0/0	8/3/0/0/0
SEMAR	0/3/24/76/50	0/0/0/5/3	0/1/1/10/30	0/0/12/13/0	0/2/9/40/16	0/0/2/8/1
Visibility of pelvic organ						
Reader 1						
AIRD 3D	43/51/22/37/0	1/2/4/1/0	0/3/6/33/0	24/1/0/0/0	10/43/12/2/0	8/2/0/1/0
SEMAR	0/0/1/89/63	0/0/0/4/4	0/0/0/8/34	0/0/0/25/0	0/0/1/43/23	0/0/0/9/2
Reader 2						
AIRD 3D	39/44/34/33/3	1/2/4/1/0	0/3/6/30/3	23/2/0/0/0	9/35/22/1/0	6/2/2/1/0
SEMAR	0/0/3/87/63	0/0/0/4/4	0/0/0/9/33	0/0/1/24/0	0/0/2/41/24	0/0/0/9/2
Visibility of muscles						
Reader 1						
AIRD 3D	83/28/35/7/0	0/5/3/0/0	3/3/29/7/0	21/4/0/0/0	49/15/3/0/0	10/1/0/0/0
SEMAR	1/4/8/87/53	0/0/0/5/3	0/1/2/10/29	0/1/2/21/1	1/2/3/45/16	0/0/1/6/4
Reader 2						
AIRD 3D	83/26/37/7/0	0/6/2/0/0	3/2/30/7/0	20/5/0/0/0	51/11/5/0/0	9/2/0/0/0
SEMAR	2/3/19/71/58	0/0/0/5/3	1/0/3/7/31	0/1/7/16/1	1/2/7/38/19	0/0/2/5/4
Visibility of vessels						
Reader 1						
AIRD 3D	10/17/46/40/40	0/0/0/0/8	0/1/0/14/27	3/6/11/3/2	7/9/28/21/2	0/1/7/2/1
SEMAR	0/1/4/45/103	0/0/0/1/7	0/0/0/2/40	0/0/2/17/6	0/1/2/24/40	0/0/0/1/10
Reader 2						
AIRD 3D	8/17/46/36/46	0/0/0/0/8	0/1/2/9/30	2/4/12/4/3	6/10/27/20/4	0/2/5/3/1
SEMAR	0/1/3/39/110	0/0/0/1/7	0/0/0/3/39	0/0/2/15/8	0/1/1/19/46	0/0/0/1/10

IF, internal fixation; *AIDR 3D*, adaptive iterative dose reconstruction algorithm; *SEMAR*, single-energy metal artifact reduction algorithm

0.81 (95% CI: 0.74 to 0.88, $P < 0.001$) and 0.85 (95% CI: 0.76 to 0.94, $P < 0.001$) for the visibility of vessels in the AIDR 3D images and SEMAR images, respectively.

In side-by-side comparisons of the reference images between the AIDR 3D and SEMAR algorithms, most SEMAR images were the same as the AIDR 3D images

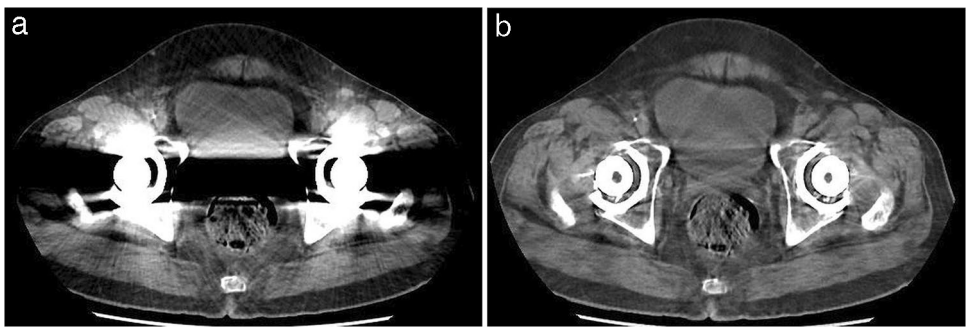

Fig. 3 A 54-year-old man with bilateral total hip arthroplasties. **a** Axial CT image reconstructed using AIDR 3D algorithm showed severe metal artifacts that masked seminal vesicles, posterior aspect of urinary bladder, anterior aspect of rectum, and adjacent muscles. **b** Axial CT image reconstructed using SEMAR algorithm improved the visibility of seminal vesicles, urinary bladder, rectum, and adjacent muscles and only mild streak artifacts were noted

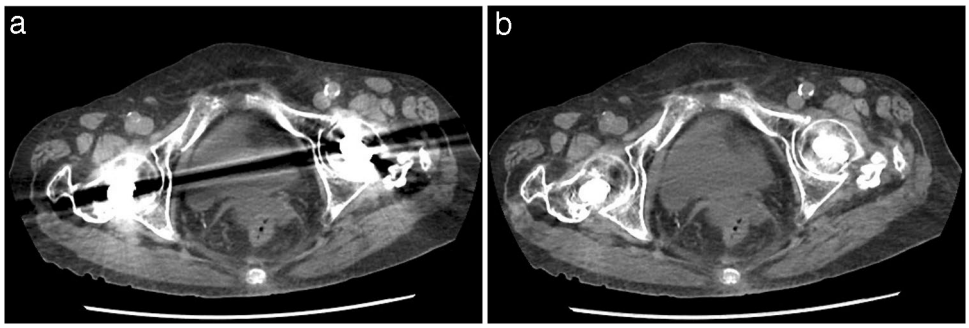

Fig. 4 A 92-year-old female with internal fixation at bilateral proximal femur. **a** Axial CT image reconstructed using AIDR 3D algorithm showed severe metal artifacts that masked urinary bladder and adjacent muscles and the overall quality scales were 1 by reader 1 and 2 by reader 2. **b** Axial CT image reconstructed using SEMAR algorithm improved the visibility of urinary bladder, rectum, and adjacent muscles and the overall quality of the scales was 5 by both readers

[reader 1: 95.4% (146/153), reader 2: 92.2% (141/153); K: 0.61 (95% CI: 0.35 to 0.87), $P < 0.001$]. Only a few SEMAR images presented slightly less quality [reader 1: 3.9% (6/153), reader 2: 6.5% (10/153)] and the peristalsis-related streak artifact was the major issue (Fig. 7). The inter-rater correlation coefficient was 0.61 (95% CI: 0.35 to 0.87).

Discussion

Results of the present study showed that the SEMAR algorithm significantly reduced metal artifacts and provided diagnostic quality images in more than 80% of the included patients. Most SEMAR images with poor quality were noted in the patients with prostheses. In the SEMAR images, no significant differences were found in the mean attenuation of soft tissues around the hardware compared with the reference images. These findings suggest that the measurements provided by the SEMAR images are reliable. To the best of our knowledge, this is the first study to evaluate the reliability of attenuation and the influence of different types of hardware in SEMAR images.

Previous studies, both phantom and clinical studies, have shown that the SEMAR algorithm significantly reduces metal artifacts [11, 14–17]. In the present study, the metal artifacts derived from hardware led to non-diagnostic quality in all images with the AIDR 3D algorithm, and the SEMAR algorithm rescued more than 80% of the images with metal artifacts in the diagnosis of soft tissues. These findings were similar to those of previous studies with pelvic CT [12–15, 18]. However, these previous studies investigated the reduction of metal artifacts in patients with hip prostheses only, and the present study investigated metal artifact reduction in patients not only with hip prostheses but also with internal fixation. The present study found that the imaging quality in patients with internal fixation only, especially unilateral fixation, was better than that in patients with prostheses, which was upheld for both AIDR 3D and SEMAR algorithms.

Although previous SEMAR studies showed not only excellent effects in reducing metal artifacts due to hip prostheses but also less variation in the CT attenuations of the bladder and muscle [13], the reliability of CT density

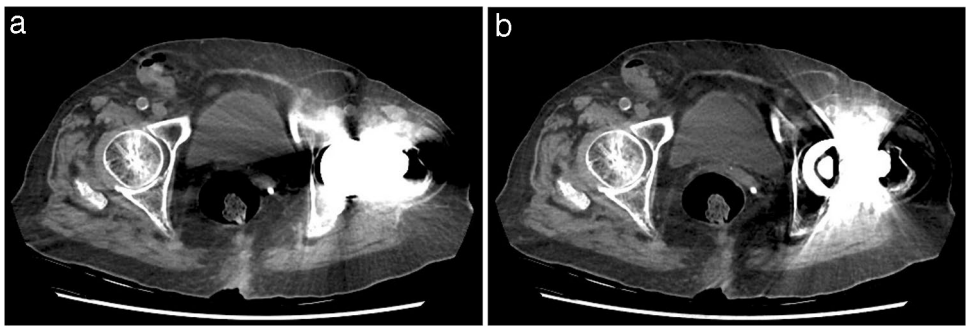

Fig. 5 A 94-year-old female with left total hip arthroplasty. **a** Axial CT image reconstructed using AIDR 3D algorithm showed severe metal artifacts that masked posterior aspect of urinary bladder, anterior aspect of rectum, and adjacent muscles and the overall quality of scales was 2 by both readers. **b** Axial CT image reconstructed using SEMAR algorithm improved the visibility of seminal vesicles, urinary bladder, rectum, and adjacent muscles and only mild streak artifacts were noted

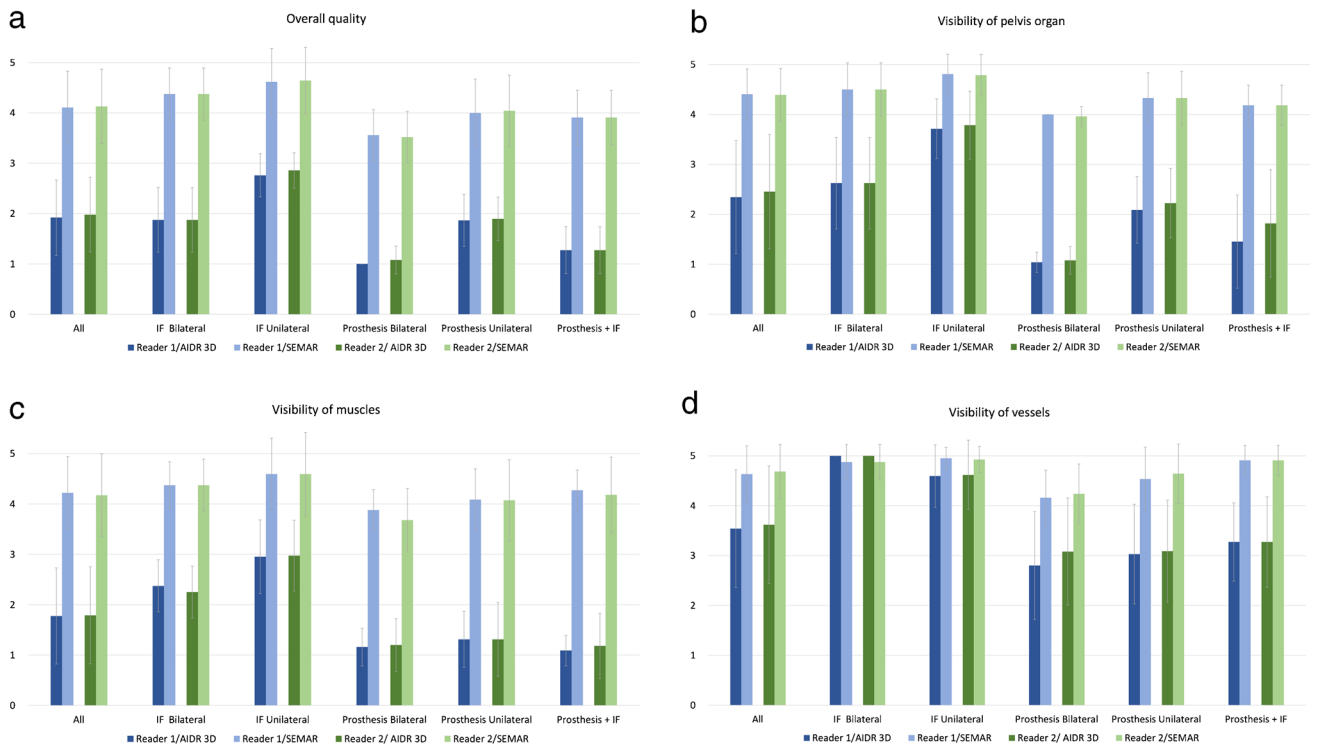

Fig. 6 Image quality scores of the images with artifacts with AIDR 3D and SEMAR algorithm: **a** overall quality; **b** visibility of pelvic organ; **c** visibility of muscles; **d** visibility of vessels

measurement at adjacent soft tissues was not well studied or discussed. The reliability of CT density measurement is important, especially in soft tissue pathology such as the differentiation between effusion, muscle, and hematoma that may influence clinical treatment decisions. In the present study, no statistically significant differences were shown between the mean densities of the urinary bladder, veins, and fat in the SEMAR images with artifacts and those in the reference images with the AIDR 3D algorithm. The results supported the good reliability of the SEMAR algorithm in CT density of the soft tissues around the metal hardware and the measured densities can be applied to the traditional evaluation criteria as well as in morphology evaluation. However, the image noises of the SEMAR images with artifacts were statistically significantly higher than those of the reference images with the AIDR 3D algorithm. These findings suggest that a region of interest should be drawn as large as possible to avoid the influence of image noise.

To evaluate the reliability of the SEMAR algorithm in the images without metal artifacts, the imaging qualities of the images with AIDR 3D and SEMAR algorithms were evaluated through side-by-side comparison, demonstrating the same quality as in most patients (92.2–95.4%). We also found no statistically significant differences when comparing the differences between the mean densities and noises of the urinary bladder, veins, and fat between the reference images of AIDR 3D and SEMAR algorithms. These results suggest that the SEMAR algorithm is reliable not

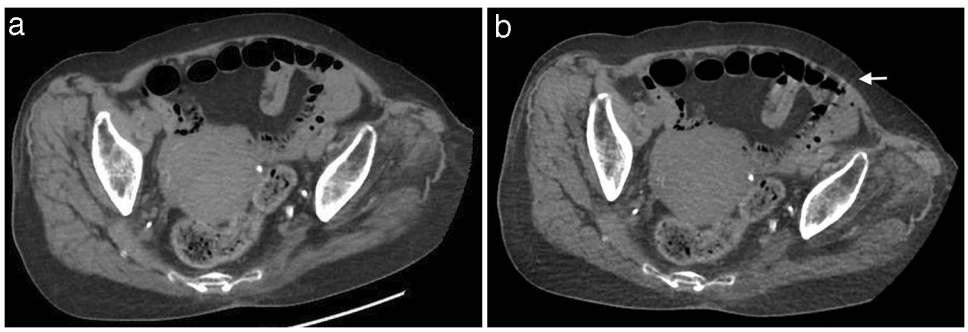

Fig. 7 An 80-year-old female with implants at left proximal femur. The $CTDI_{vol}$ of AIDR 3D image (**a**) was 9.9 mGy and SEMAR image (**b**) was 8.7 mGy. The SEMAR image (**b**) presented increased image noise and tiny peristalsis-related streak artifact (arrow) at left anterior abdominal wall and adjacent bowel loops

only in images with metal artifacts but also in the images without metal artifacts.

In the present study, the $CTDI_{vol}$ of the images with SEMAR algorithm was statistically significantly lower in patients with unilateral fixation than in those with the AIDR 3D algorithm, and no significant differences were found between the AIDR 3D and SEMAR algorithms in patients with prostheses or bilateral fixation. In our CT protocol setting, the tube current (mA) was determined by automatic exposure control (AEC) and the reconstruction algorithm was one of the influencing factors. We supposed that the better reduction of metal artifacts caused by unilateral fixation may be the major cause of a lower tube current. Although no similar study has compared the radiation dose between these two algorithms, previous SEMAR study has shown that the radiation doses in the patients with bilateral prostheses were higher than those in the patients with unilateral prosthesis [15]. According to these findings, we supposed that the reduction ability for metal artifacts contributes not only to the image quality but also to the radiation dose.

The present study has a few limitations that warrant discussion. First, the study was retrospective and discussed the imaging quality of the SEMAR algorithm in patients with metallic devices. However, we lacked specific information about the materials of the metallic devices, such as titanium, steel, or other metals, and could not verify the influence of these different materials. Second, the sample size was small, especially in groups of bilateral fixation and arthrography + fixation. Third, the enrolled subjects had no significant disease of the pelvic and periarticular organs, so the diagnostic accuracy of AIDR 3D and SEMAR algorithms could not be evaluated.

In conclusion, the SEMAR algorithm provides significant reduction of metal artifacts, more in patients with internal fixations than in patients with prostheses. The attenuation of soft tissues in CT with the SEMAR algorithm is reliable not only in the images with metal artifacts but also in the images without metal artifacts.

Acknowledgements The authors thank the Division of Medical Statistics and Bioinformatics, Department of Medical Research, Kaohsiung Medical University Hospital, Kaohsiung Medical University, for assistance with this study.

Declarations

Ethics approval This study was approved by the Institutional Review Board of Kaohsiung Medical University Chung-Ho Memorial Hospital (IRB No: KMUHIRB-E(1)-20190447). Because of the retrospective nature, the requirement of informed consent was waived.

Conflict of interest The authors declare no competing interests.

References

1. Veronese N, Maggi S. Epidemiology and social costs of hip fracture. Injury. 2018;49(8):1458–60.
2. Bhandari M, Swiontkowski M. Management of acute hip fracture. N Engl J Med. 2017;377(21):2053–62.
3. Deshmukh S, Omar IM. Imaging of hip arthroplasties: normal findings and hardware complications. Semin Musculoskelet Radiol. 2019;23(2):162–76.
4. Vande Berg B, Malghem J, Maldague B, Lecouvet F. Multi-detector CT imaging in the postoperative orthopedic patient with metal hardware. Eur J Radiol. 2006;60(3):470–9.
5. Katsura M, Sato J, Akahane M, Kunimatsu A, Abe O. Current and novel techniques for metal artifact reduction at CT: practical guide for radiologists. Radiographics. 2018;38(2):450–61.
6. Wellenberg RHH, Hakvoort ET, Slump CH, Boomsma MF, Maas M, Streekstra GJ. Metal artifact reduction techniques in musculoskeletal CT-imaging. Eur J Radiol. 2018;107:60–9.
7. Goodsitt MM, Christodoulou EG, Larson SC. Accuracies of the synthesized monochromatic CT numbers and effective atomic numbers obtained with a rapid kVp switching dual energy CT scanner. Med Phys. 2011;38(4):2222–32.
8. Yu L, Leng S, McCollough CH. Dual-energy CT-based monochromatic imaging. AJR Am J Roentgenol. 2012;199(5 Suppl):S9-s15.
9. Meinel FG, Bischoff B, Zhang Q, Bamberg F, Reiser MF, Johnson TR. Metal artifact reduction by dual-energy computed tomography using energetic extrapolation: a systematically optimized protocol. Invest Radiol. 2012;47(7):406–14.
10. Lewis M, Reid K, Toms AP. Reducing the effects of metal artefact using high keV monoenergetic reconstruction of dual energy CT (DECT) in hip replacements. Skeletal Radiol. 2013;42(2):275–82.
11. Grandmougin A, Bakour O, Villani N, et al. Metal artifact reduction for small metal implants on CT: which image reconstruction algorithm performs better? Eur J Radiol. 2020; 127:108970.
12. Barreto I, Pepin E, Davis I, et al. Comparison of metal artifact reduction using single-energy CT and dual-energy CT with various metallic implants in cadavers. Eur J Radiol. 2020; 133:109357.
13. Yasaka K, Maeda E, Hanaoka S, Katsura M, Sato J, Ohtomo K. Single-energy metal artifact reduction for helical computed tomography of the pelvis in patients with metal hip prostheses. Jpn J Radiol. 2016;34(9):625–32.
14. Sonoda A, Nitta N, Ushio N, et al. Evaluation of the quality of CT images acquired with the single energy metal artifact reduction (SEMAR) algorithm in patients with hip and dental prostheses and aneurysm embolization coils. Jpn J Radiol. 2015;33(11):710–6.
15. Gondim Teixeira PA, Meyer JB, Baumann C, et al. Total hip prosthesis CT with single-energy projection-based metallic artifact reduction: impact on the visualization of specific periprosthetic soft tissue structures. Skeletal Radiol. 2014;43(9):1237–46.
16. Kidoh M, Utsunomiya D, Ikeda O, et al. Reduction of metallic coil artefacts in computed tomography body imaging: effects of a new single-energy metal artefact reduction algorithm. Eur Radiol. 2016;26(5):1378–86.
17. Chou R, Li JH, Ying LK, Lin CH, Leung W. Quantitative assessment of three vendor's metal artifact reduction techniques for CT imaging using a customized phantom. Comput Assist Surg (Abingdon). 2019;24(sup2):34–42.
18. Asai S, Sobue Y, Asai N, et al. Computed tomography evaluation of the periacetabular gap of a porous tantalum acetabular component. Nagoya J Med Sci. 2019;81(1):159–63.